Sensors and Actuators A 193 (2013) 13–24

Contents lists available at SciVerse ScienceDirect

Sensors and Actuators A: Physical

journal homepage: www.elsevier.com/locate/sna

Piezoelectric properties of PVDF/MWCNT nanofiber using near-field electrospinning

Z.H. Liu [a,b,c], C.T. Pan [a,b,*], L.W. Lin [d], H.W. Lai [a]

[a] Department of Mechanical and Electro-Mechanical Engineering, National Sun Yat-Sen University, Kaohsiung 80424, Taiwan
[b] Center for Nanoscience & Nanotechnology, National Sun Yat-Sen University; National Science Council Core Facilities Laboratory for Nano-Science and Nano-Technology in Kaohsiung-Pingtung area, Taiwan
[c] Electronics and Optoelectronics Research Laboratories, Industrial Technology Research Institute, Hsinchu 310, Taiwan
[d] Department of Mechanical Engineering and Berkeley Sensor and Actuator Center, University of California, Berkeley, CA 94720, United States

ARTICLE INFO

Article history:
Received 16 September 2012
Received in revised form 7 January 2013
Accepted 7 January 2013
Available online 11 January 2013

Keywords:
Actuation
Coupled field analysis
Electrospinning
Piezoelectric nanofiber
PVDF/MWCNT

ABSTRACT

This study reports the use of near-field electrospinning to fabricate polyvinylidene fluoride (PVDF) piezoelectric nanofibers mixed with multiwalled-carbon nanotubes (MWCNT). This study also investigates the mechanical strength and piezoelectric characteristics of a single PVDF/MWCNT nanofiber. The morphology and polarization intensity of piezoelectric fiber can be controlled by adjusting the traveling velocity of the *X–Y* stage, the DC voltage, and the gap between the needle and collection plate. The optimal parameters of the PVDF solution, such as the PVDF powder weight percentage and MWCNT content, were also determined. X-ray diffraction (XRD) analysis shows a high diffraction peak at $2\theta = 20.8^{\circ}$ in the piezoelectric crystal β-phase structure. ANSYS finite element analysis (FEA) software with coupled field analysis was used to realize piezoelectric actuation behavior of the PVDF fibers. A nano-indentation test (NanoIndenter XP System, MTS co.) was used to investigate Young's modulus of the PVDF fiber. Finally, the fixed–fixed beam structures of PVDF composite fibers were tested using a DC voltage supply. Comparing the polarized fiber with non-polarized fibers, the measurement of the center displacements as a function of electric field was conducted and characterized.

1. Introduction

Polyvinylidene fluoride (PVDF) is a popular piezoelectric polymer because of its high flexibility, biocompatibility, and low cost. These features make PVDF attractive for energy conversion applications involving microelectric-mechanical devices, electromechanical actuators, and energy harvesters [1]. Several researchers have studied PVDF actuators in the form of thin film [2–4]. However, only a few studies have examined single PVDF fibers [5]. The current study presents a method of controllable electrospinning based on a new type of near-field electrospinning (NFES). This method can potentially be scaled down to the nanometer scale and form any shape for various sensing and actuation applications. The main advantages of NFES-formed PVDF/MWCNT composite fibers are their excellent properties, including structure scalability, greater flexibility, and greater piezoelectric strain constant ($d_{33} \sim -57.6$ pm/V) [6] compared with commercially available PVDF thin films ($d_{33} \sim -15$ pm/V) [7].

PVDF is a semicrystalline polymer consisting of four crystalline phases: α, β, γ, and δ. The non-polar α phase is most commonly found in commercially available films. Because the dipole moments in this phase have a random orientation, they cancel each other out. The β phase has dipole moments pointing in the same direction; thus, the β phase is responsible for the piezoelectric properties of PVDF polymer. Yee et al. announced a method of electrospinning PVDF fiber [8]. In a typical electrospinning process, fibers are emitted from a Taylor cone when the solution is subjected to a high-voltage electrostatic field [9]. As electrostatic force stretches the fiber, it bends into a complex path, causing chaotic whipping of the fiber jet [10]. As the fibers form in the electrospinning process, they are unstable in nature. Highly aligned fibers are therefore difficult to achieve using this method. Fennessey and Kim investigated different techniques to align electrospun fibers using a rotating collector [11,12], and Wang [13] modified the electric field. Other researchers improved the electrospinning process with fundamental physics and chemistry for better control [14].

A direct-write electrospinning technique using NFES [15,16] was developed to achieve controllable fiber deposition for various materials. Unlike the conventional electrospinning process, NFES only needs a small electric field to produce continuous fibers with fine diameters. Chang et al. reported electrospinning PVDF fibers

* Corresponding author at: Department of Mechanical and Electro-Mechanical Engineering, National Sun Yat-Sen University, No. 70 Lien-hai Road, Kaohsiung 80424, Taiwan. Tel.: +886 7 5252000x4239, fax: +886 7 5254299.
E-mail address: panct@mail.nsysu.edu.tw (C.T. Pan).

0924-4247/$ – see front matter © 2013 Elsevier B.V. All rights reserved.
http://dx.doi.org/10.1016/j.sna.2013.01.007

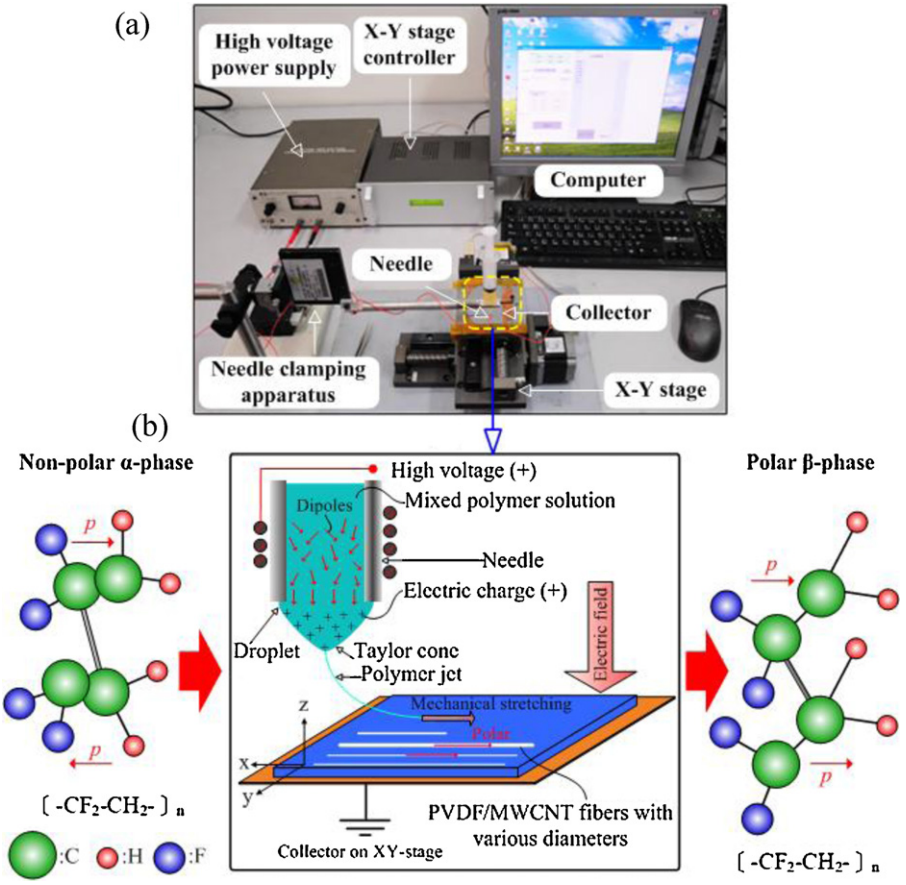

Fig. 1. (a) The photo of near-field electrospinning setup. (b) Direct-write PVDF fiber process with in situ poling: the dipoles in the non-polar, α-phase PVDF could be stretched and oriented by a high electrical field with in situ strong mechanical stretching to become the polar.

with high energy conversion efficiency for power handheld electronics through body movements [17]. This approach can be used to form PVDF fibers with in situ electrical poling. Therefore, electrospinning a PVDF solution can transform the non-polar α phase into the polar β phase [8]. Furthermore, adding modified carbon nanotubes (CNTs) to reinforce PVDF fibers can enhance the crystallinity of the β phase. Zhang et al. [18] showed that CNTs can facilitate the growth of the crystalline β phase in PVDF composite fiber, enhancing piezoelectric properties.

This study demonstrates the controllability of electrospun PVDF fibers using NEFS. This method reduces the electrode-to-collector distance, which is typically on the order of 10 cm in the conventional electrospinning process, to less than 1 mm. This is a powerful method to direct-write PVDF fibers with high controllability. The optimal parameters of the PVDF solution, such as weight percentage of the PVDF powder and multiwalled carbon nanotubes (MWCNTs), were determined to obtain the optimal β-crystalline structure and surface morphology. Under the strong extensional force in NFES process, the unique crystalline structures of the PVDF/MWCNT in orderly aligned PVDF fibers resulted by the cooperative orientation of the MWCNTs and PVDF chains were aligned in sequence along the fiber axis, which promotes the nucleation of highly oriented β-form extended-chain crystallites at the interface.

X-ray diffraction (XRD) analysis of the PVDF composite fibers shows a high diffraction peak at $2\theta = 20.8^{\circ}$ in the piezoelectric crystal β-phase structure. A single piezoelectric PVDF fiber was simulated using ANSYS FEA commercial software to determine its actuation behavior under an external electric field. The actuation property was tested using a DC voltage supply.

2. Analysis of PVDF fiber-based flexible piezoelectric actuator

2.1. Near-field electrospinning process

Fig. 1 shows the experimental NFES setup, which includes a needle, high-voltage power supply, collector (silicon wafer), *X*–*Y* motion stage (controlled by *X*–*Y* stage controller through a computer), and needle holder. The inner diameters of needles ranged from 0.15 to 0.3 mm. The anode of the high-voltage power supply was connected to the needle holder, and the silicon wafer was grounded as a collector. A high-voltage 1200 V formed a high potential between the needle and the collector. The collector was installed on an *X*–*Y* stage with a motion speed of 20–100 mm/s and a travel distance of 50 mm, respectively. The gap between the needle and the collector was 0.5–1 mm, and the route of the collector mounted on the *X*–*Y* stage was controlled by a programmed path. Under a high electric potential, the droplet overcame the surface tension of the solution and was ejected from the needle tip, spinning an extremely fine PVDF fiber out on the collector. The applied electric field generated sufficient electrostatic force to deform the polymer meniscus into a conical shape (Taylor cone) and subsequently induce a polymer jet from the tip of the Taylor cone. In the preparation of PVDF solution, dimethyl sulfoxide (DMSO) uses as the solvent for PVDF powder ($Mw = 534{,}000$), with acetone and fluorosurfactant (ZONYL®UR) to improve the evaporation rate and reduce the surface tension of PVDF solution, respectively. The proper percentage of MWCNT was dispersed in DMSO, and PVDF was dispersed in acetone simultaneously. The MWCNT–DMSO solution was sonicated for at least 1 h to break

Table 1
The composition of the PVDF solutions used in this study, including weight percentage of PVDF powder, solvent, Zonyl®UR, and MWCNT.

PVDF		Solvent (DMSO:acetone)		Zonyl®UR		MWCNT	
Weight ratio (PVDF/solvent) (wt%)	Weight (g)	DMSO (g)	Acetone (g)	Weight ratio (wt%)	Weight (g)	Weight ratio	Weight (g)
16	0.8	2.5	2.5	5	0.3	0	None
18	0.9	2.5	2.5	5	0.3	0	None
18	0.9	2.5	2.5	5	0.3	0.01 wt%	0.005
18	0.9	2.5	2.5	5	0.3	0.03 wt%	0.015
18	0.9	2.5	2.5	5	0.3	0.05 wt%	0.025
20	1	2.5	2.5	5	0.5	0	None

Table 2
Material properties of piezoelectric PVDF fiber.

Density (kg/m^3)	1780	Poisson ratio	0.39

possible agglomerates. PVDF, MWCNT–DMSO solutions, and surfactant were mixed. The mixed solution was completely sealed in a container to prevent evaporation effects at room temperature. Table 1 shows the PVDF and MWCNT concentrations used in this study.

2.2. Model solution of single PVDF fiber

Fig. 2 shows the geometry and boundary conditions of a single PVDF fiber, where D is the diameter of the fiber, L is the original length, L is the change in fiber length, S_3 is the internal strain along the fiber axis, D_c is the center displacement, E_3 is the applied electric field, P is the polarization, and V_3 is the input voltage applied on the fixed end.

Eqs. (1) and (2) are e-form piezoelectric constitutive equations for the d_{33} conversion mode. The terms T_3 and D_3 are the internal stress and electric displacement, ψ_3 is the electric potential, c_{33}^E is the mechanical stiffness constant under a constant electric field, e_{33} is the piezoelectric stress constant, and ε_{33}^S is the permittivity under a constant strain. Table 2 shows the material properties of piezoelectric PVDF fiber. Several important parameters associated with the piezoelectricity of PVDF fiber are listed in Appendix.

$$T_3(S,E) = c_{33}^E S_3 - e_{33}E_3 = c_{33}^E S_3 + e_{33}\frac{\partial \psi_3}{\partial z} \tag{1}$$

$$D_3(T,E) = e_{33}S_3 + \varepsilon_{33}^S E_3 \tag{2}$$

According to the boundary conditions of the fixed–fixed PVDF fiber structure, the transverse and shear effect are negligible. Therefore, the actuation equation of PVDF fiber can be simplified as (3).

Eq. (4) shows the relationship between the internal strain and displacement (w) in the z-axis direction, where ρ is the density of the PVDF fiber. Eqs. (1) and (4) are combined. The actuation equation can be expressed by (5). In addition, ψ_3 is a function of w and the position of the z-axis (z).

$$\frac{\partial T_3}{\partial z} = \rho\frac{\partial^2 w}{\partial t^2} \tag{3}$$

$$S_3 = \frac{\partial w}{\partial z} \tag{4}$$

$$\frac{\partial^2 w}{\partial z^2} - \frac{e_{33}}{c_{33}^E}\frac{\partial^2 \psi_3}{\partial z^2} = \frac{\rho}{c_{33}^E}\frac{\partial^2 w}{\partial t^2}, \quad \left(\frac{\partial^2 \psi_3}{\partial z^2} \neq 0\right) \tag{5}$$

The electric and mechanical boundary conditions were set as $\Psi_3|_{z=\pm L/2} = \pm V_3$ and $T_3|_{z=\pm L/2} = 0$ (or $\delta w/\delta z|_{z=\pm L/2} = e_{33}/c_{33}^E \cdot \delta\Psi_3/\delta z|_{z=\pm L/2}$), respectively. This study describes the electric displacement equation and quasi-static equation as (6) and (7), respectively. Then, (5) can be revised as (8).

$$D_3(T,E) = e_{33}\frac{\partial w}{\partial z} + \varepsilon_{33}^S\frac{\partial \psi_3}{\partial z}; \quad \varepsilon_{33}^S = \varepsilon_{33}^T(1-k_{d_{33}}^2) \tag{6}$$

$$\frac{\partial^2 \psi_3}{\partial z^2} = -\frac{e_{33}}{\varepsilon_{33}^S}\frac{\partial^2 w}{\partial z^2}; \quad \left(\text{as asssuming}\frac{\partial D_3}{\partial z} = 0\right) \tag{7}$$

$$\frac{\partial^2 w}{\partial z^2} = \frac{\rho}{c_{33}^E(1-k_{e_{33}}^2)}\frac{\partial^2 w}{\partial t^2}; \quad k_{e_{33}}^2 = \frac{e_{33}^2}{c_{33}^E\varepsilon_{33}^S} \tag{8}$$

The solution of the displacement can be represented as (9). Thus, (8) can be rearranged as (10), where ω is the angular frequency.

$$w(z,t) = \bar{w}(z)e^{j\omega t} \tag{9}$$

$$\frac{\delta^2 \bar{w}}{\delta z^2} + \lambda^2 \bar{w} = 0; \quad \lambda^2 = \frac{\rho\omega^2}{c_{33}^E(1-k_{e_{33}}^2)} \tag{10}$$

The general solution of displacement can be solved using (11). Eq. (12) shows that the strain solution as a function of k_{e33} is directly

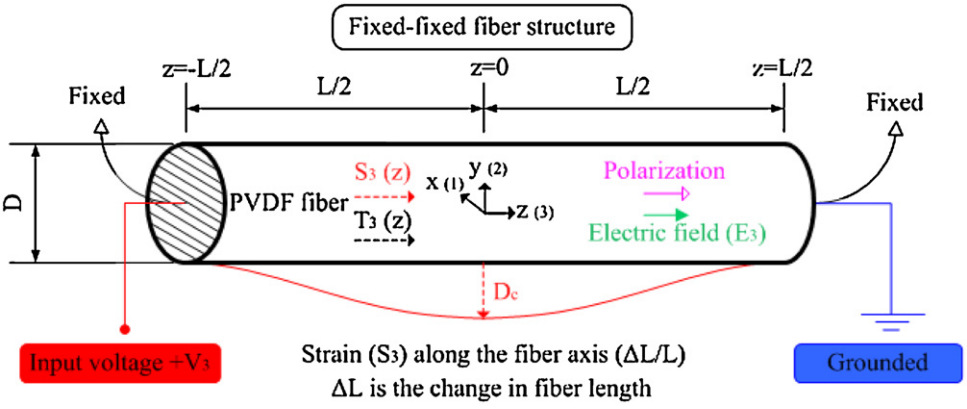

Fig. 2. The central part of an electrospun PVDF fiber with a $-d_{33}$ piezoelectric constant after applying an external electric field along the fiber length. A positive electric field ($+E$) is defined as having the same direction as the polarization, and a negative electric field ($-E$) is defined as having the opposite direction of polarization.

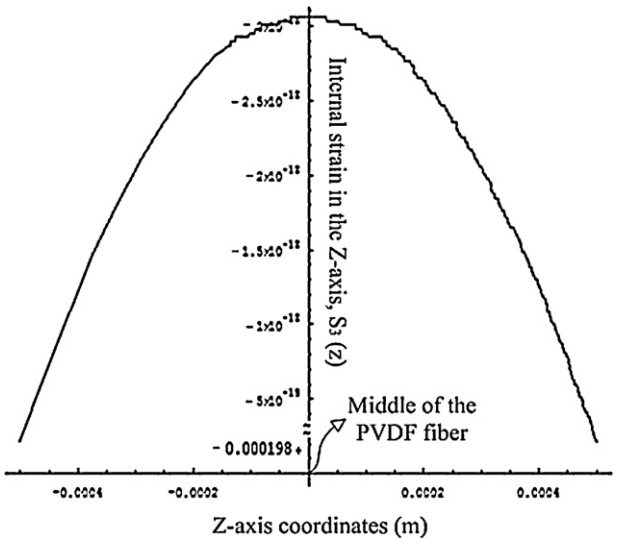

Fig. 3. The internal strain in the z-axis of PVDF fiber under a voltage of +1.5 kV.

proportional to V_3. Because PVDF fiber has a negative piezoelectric stress constant ($-e_{33}$), $+V$ causes compressive strain ($-S_3$) along the fiber axis and $-V$ causes tensile strain ($+S_3$). Fig. 3 shows the model solution of the strain along the z-axis under +1.5 kV. Results show that a maximum compression strain appears in the middle of the fixed–fixed PVDF fiber structure.

$$\bar{w}(z) = \frac{e_{33}V_3 \quad \sin(2az/L)}{c_{33}^E a(1-k_{e_{33}}^2) \quad \cos \quad a[1-(k_{e_{33}}^2/(1-k_{e_{33}}^2))(\tan \quad a/a)]}; \qquad a = \frac{L\lambda}{2} \tag{11}$$

$$S_3(z) = \frac{d\bar{w}(z)}{dz} = \frac{2e_{33}V_3\cos(2az/L)/[c_{33}^E(1-k_{e_{33}}^2) \quad \cos a]}{L(1-(k_{e_{33}}^2/(1-k_{e_{33}}^2))(\tan \quad a/a))} \tag{12}$$

This study uses an analytical formula analysis (13) [19,20] to determine the vertical deformation induced by the buckling effect under a positive electric field. The center displacement (D_c) can then be predicted using (14).

$$S_3(z) = 2.44\left(\frac{D_c}{L}\right)^2 \tag{13}$$

$$D_c^2 = \frac{2Le_{33}V_3\cos(2az/L)/[c_{33}^E(1-k_{e_{33}}^2)\cos a]}{2.44L(1-(k_{e_{33}}^2/(1-k_{e_{33}}^2))(\tan a/a))} \tag{14}$$

The buckling effect of the fixed–fixed PVDF fiber structure produced a repulsive force (R) and moment (M) near the fixed end, and an electrostatic attraction force (F) on the surface of the PVDF fiber. Experimental results explain this phenomenon. Fig. 4 shows a schematic diagram of the fixed–fixed PVDF fiber structure and its actuation properties after applying an electric field to the fixed end. After the PVDF/MWCNT fiber was formed on a wafer collector, a single fiber was glued to the insulation epoxy/PI film and copper foil electrodes. Silver glue was then coated on the fixed end of the PVDF fiber to reduce the electrostatic effect [6].

3. Experimental details

3.1. Optimal parameters of near-field electrospinning PVDF/MWCNT nanofiber

As Fig. 5(a) shows, the internal diameter of the needle was 0.25 mm. When the droplet overcame the surface tension of the solution (Fig. 5(b)), a PVDF fiber was spun from the Taylor cone tip (with a needle-to-collector distance of approximately 1 mm), and the droplet volume gradually decreased (Fig. 5(c)). Various patterns were collected on the collector to demonstrate the controllability of NFES using a programmable path X–Y stage. PVDF fibers with a diameter of 0.7–1 μm were spun on the collector (Fig. 6(a)). Fig. 6(b) shows English words and woven structures made of PVDF composite fiber. The PVDF fiber grating patterns were observed using a scanning electron microscope (SEM), showing that fibers were not bonded together because the solvent inside the PVDF fiber had completely evaporated (Fig. 6(c)). The time delay of the X–Y stage made the polymer jet unstable, creating spirals in the corners (Fig. 6(d)).

The diameter of PVDF nanofibers can be adjusted by controlling various parameters, including the internal diameter of the needle, the electric field, the X–Y stage speed, the PVDF solution concentration, and the MWCNT concentration. To determine the influence of these parameters on PVDF nanofiber diameter, we changed only one parameter at one time during NFES. The needle-to-collector distance was fixed at 1 mm for various needle sizes of 0.15, 0.23, 0.28, and 0.3 mm. The DC voltage, X–Y stage speed, and PVDF solution concentration were fixed at 900 V, 60 mm/s, and 18 wt%, respectively. Fig. 7 shows the relationship between the internal diameter of the needle and the diameter of the PVDF fibers. Results show that the PVDF fiber diameter depends on the needle size. With a 0.3 mm needle, when the droplet overly accumulated

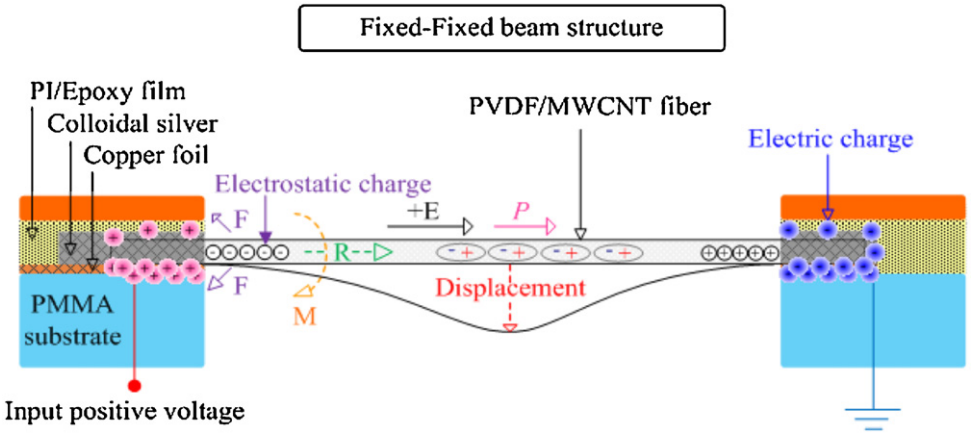

Fig. 4. Schematic diagram of the fixed–fixed beam structure: deformation of fiber under an electric field ($+E$) with two different effects: (1) inverse piezoelectric effect of repulsive force (R) and moment (M) and (2) electrostatic effect of electrostatic attraction force (F).

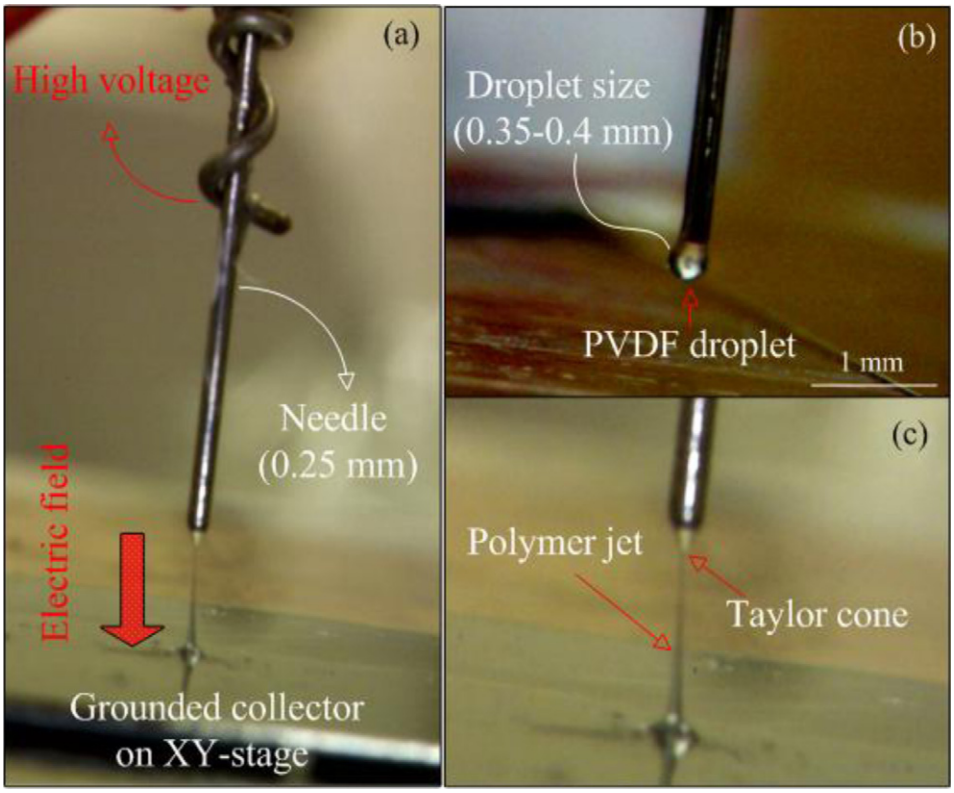

Fig. 5. Near-field electrospinning PVDF fiber process.

on the tip, there was not enough space between the Taylor cone tip and the collector. Thus, a large droplet would directly drop on the collector, blocking the spinning route. When the needle size was 0.15 mm, the PVDF solution was difficult to spin because of high viscous resistance on the internal wall of the needle. Thus, experiments showed that the needle size of 0.23 mm produced a stable jet of polymer solution during the electrospinning process.

The needle-to-collector distance was fixed at 1 mm for various electric fields of 0.8, 1, 1.2, and 1.5 kV/mm. The needle size, *X*–*Y* stage speed, and PVDF solution concentration were fixed at 0.23 mm, 80 mm/s, and 18 wt%, respectively. Fig. 8 shows the relationship between the electric field and the diameter of the PVDF fibers, demonstrating a linear relationship between the fiber diameter and applied electric field. Under a higher electric field, both the Taylor cone size and polymer jet diameter increased. This resulted in thicker fibers, and made it difficult to control the fiber diameter. In continuous NFES, the effect of the Columbic repulsion force in the polymer jet can be reduced by decreasing the needle-to-collector distance. In this case, there was insufficient space between the Taylor cone tip and collector to whip the fibers for stretching the fibers, compared with the conventional electrospinning process.

The needle-to-collector distance was fixed at 1 mm for various *X*–*Y* stage speeds of 30, 50, 70, and 90 mm/s. The needle size, DC voltage, and PVDF solution concentration were fixed at 0.23 mm, 1200 V, and 18 wt%, respectively. Fig. 9 shows the relationship between the *X*–*Y* stage speed and the diameter of the PVDF fibers. Results show that the PVDF fiber diameter is inversely proportional to the *X*–*Y* stage speed. If the *X*–*Y* stage speed falls below 30 mm/s, the polymer jet becomes unstable and forms spirals on the collector. When the *X*–*Y* stage moves at 80–90 mm/s, the diameter of the PVDF fibers becomes less than 5 μm without discontinuity.

The needle-to-collector distance was fixed at 1 mm for various PVDF solution concentrations of 16, 18, and 20 wt%. The needle size, DC voltage, and *X*–*Y* stage speed were fixed at 0.23 mm, 900 V, and 80 mm/s, respectively. Fig. 10 shows the relationship between the solution concentration and the diameter of the PVDF fibers, indicating that the fiber diameter is inversely proportional to the solution concentration. When the solution concentration is lower than 16 wt%, the NFES process becomes discontinuous because of an unsteady solution flow rate. This leads to the formation of PVDF fiber with a non-uniform fiber diameter. Therefore, the concentration of the PVDF solution was set at 18 wt% to obtain the desired viscosity and surface tension property of the PVDF solution.

Finally, MWCNTs were added to the PVDF solution to enhance the crystallinity of the β phase in PVDF fibers. The needle-to-collector distance was fixed at 1 mm for various MWCNT concentrations of 0, 0.01, 0.03, and 0.05 wt%. The DC voltage, *X*–*Y* stage speed, and PVDF solution concentration were fixed at 1200 V, 80 mm/s, and 18 wt%, respectively. Fig. 11 shows the relationship between MWCNT concentration and the diameter of the PVDF fibers. Results show that the PVDF fiber diameter is slightly inversely proportional to the MWCNT concentration.

The NFES process produced the desired viscosity and surface tension property with a 0.03 wt% MWCNT content in the PVDF solution, yielding PVDF/MWCNT fibers with a uniform diameter. When the MWCNT concentration ncreased to 0.05 wt%, the solution was difficult to eject because of a higher viscous resistance. Unsteady solution flow in the NFES process then led to a non-uniform fiber diameter.

This study also uses a nano-indentation test (NanoIndenter XP System, MTS co.) to investigate Young's modulus of the PVDF fiber with 0.03 wt% MWCNT. The nano-indentation technique can be used to analyze load–displacement curves to obtain critical information on mechanical properties. Results show that Young's modulus of PVDF fiber is 0.26 GPa. After adding 0.03% of MWCNT, the mechanical properties increase by 19.2% to 0.31 GPa. Therefore, adding MWCNT to PVDF fibers can improve their mechanical properties and enhance their tensile strength.

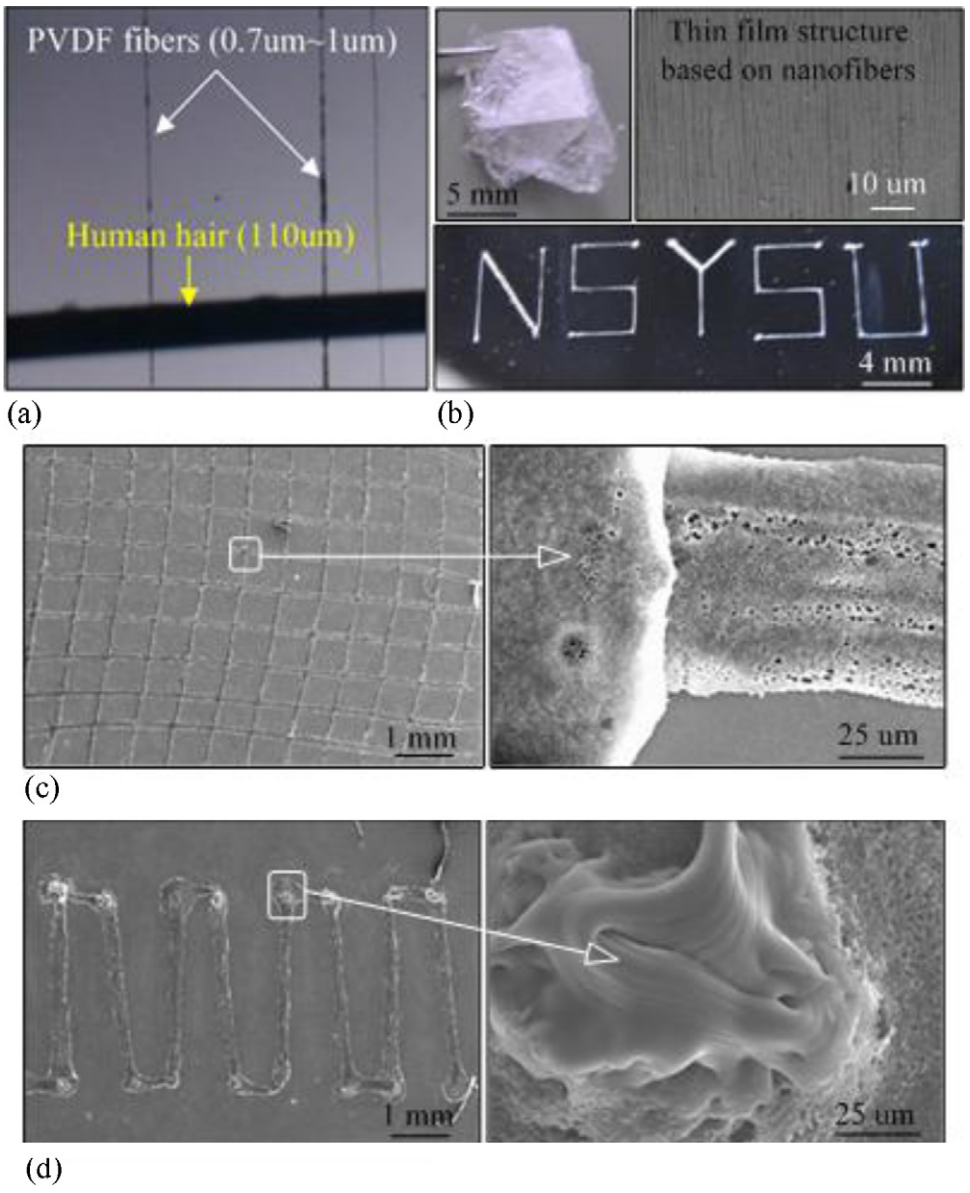

Fig. 6. The diameter of PVDF fibers and other patterns: (a) PVDF fibers with a diameter of 0.7–1 μm spun on a collector, (b) words and woven structures made of PVDF piezoelectric fibers, (c) SEM observation of grating structures, and (d) the heap of unstable polymer jet in the corner.

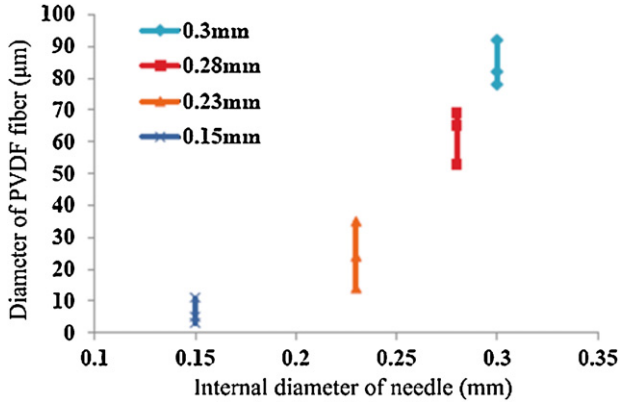

Fig. 7. The relationship between the internal diameter of the needle and the diameter of PVDF fibers (DC voltage 900 V, *X*–*Y* stage speed 60 mm/s, and PVDF solution concentration 18 wt%).

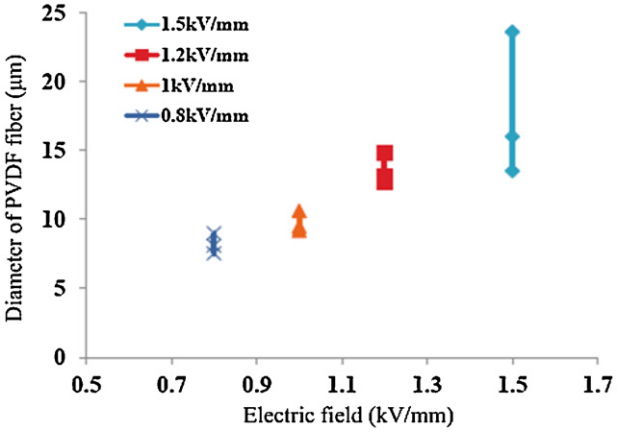

Fig. 8. Relationship between the electric field and the diameter of PVDF fibers (needle size 0.23 mm, *X*–*Y* stage speed 80 mm/s, and PVDF solution concentration 18 wt%).

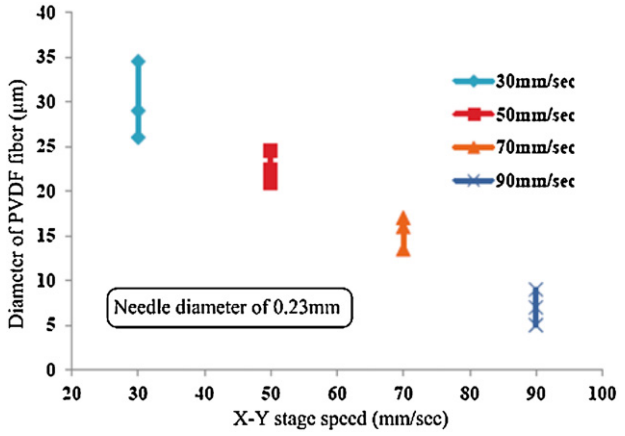

Fig. 9. The relationship between the *X–Y* stage speed and the diameter of the PVDF fibers (needle size 0.23 mm, DC voltage 1200 V, and PVDF solution concentration 18 wt%).

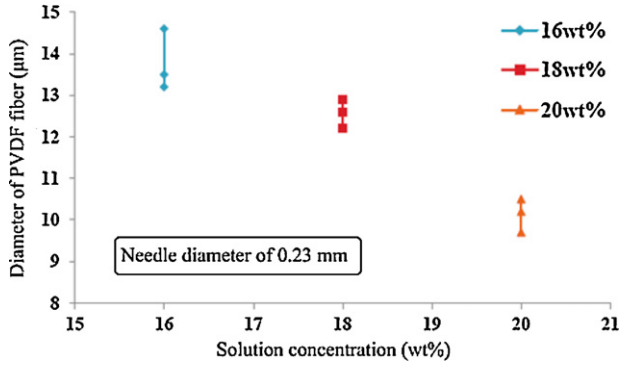

Fig. 10. The relationship between solution concentration and the diameter of PVDF fibers (needle size 0.23 mm, DC voltage 900 V, and *X–Y* stage speed 80 mm/s).

3.2. SEM observations of PVDF/MWCNT composite fibers

Distribution of MWCNTs in the PVDF solution and interfacial adhesion between MWCNTs and PVDF chains are two major factors to determine the reinforcement effect of MWCNTs in the orderly aligned PVDF fibers, such as crystallization, mechanical behaviors and piezoelectricity [22]. The MWCNT content also affects the morphology of the electrospun PVDF composite nanofibers. Fig. 12 shows SEM images of PVDF/MWCNT crystal structures. MWCNTs and PVDF chains were aligned along the poling and stretching direction. Fig. 13 shows that some tiny pores formed on the surface of the 0.03 wt% MWCNT fibers as they dried. Defects such as holes and voids can be observed on solidified PDVF fibers. These are caused by a great amount of volatile acetone in the PVDF solution. Therefore, when the baking temperature is set to 50 °C, the acetone evaporated quickly, and the PVDF solution cannot reflow to fill up the holes and voids in time. Compared with PVDF thin film, PVDF/MWCNT fiber produced by the NFES process has a higher degree of crystallinity and better orientation of molecular chains [21]. When MWCNT in PVDF solution increases to 0.05 wt%, the resulting fibers exhibit numerous cracks and large pores on the surface (Fig. 14). A non-uniform diameter is also apparent, and may result from an unsteady solution flow rate in the initial electrospinning process.

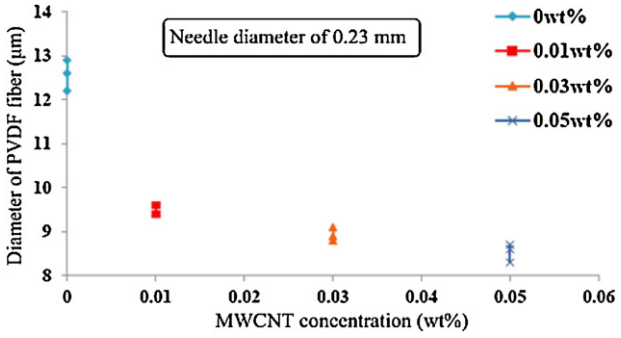

Fig. 11. The relationship between the MWCNT concentration and the diameter of PVDF fibers (needle size 0.23 mm, DC voltage 1200 V, *X–Y* stage speed 80 mm/s, and PVDF solution concentration 18 wt%).

3.3. XRD analysis of PVDF composite fibers

This study uses XRD observation of PVDF composite fibers to verify the in situ electric poling and mechanical stretching effects of the NFES process. Fig. 15 shows the XRD diffraction patterns of PVDF fiber under various electric fields. Results show that when a higher electric field of 1200 V/mm is applied in the NFES process, the β-crystalline structure of the PVDF fibers increased by approximately 53% compared with an electric field of 600 V/mm. This is because a higher electric field produces a completely different arrangement of the polarity direction of the PVDF fiber, facilitating the growth of the crystalline structure (diffraction peak at $2\theta = 20.8^{\circ}$). Fig. 16 shows that when different concentrations of PVDF solution were prepared, the intensity of the β phase did not change significantly. The intensity of the β phase increased by 25–28% after

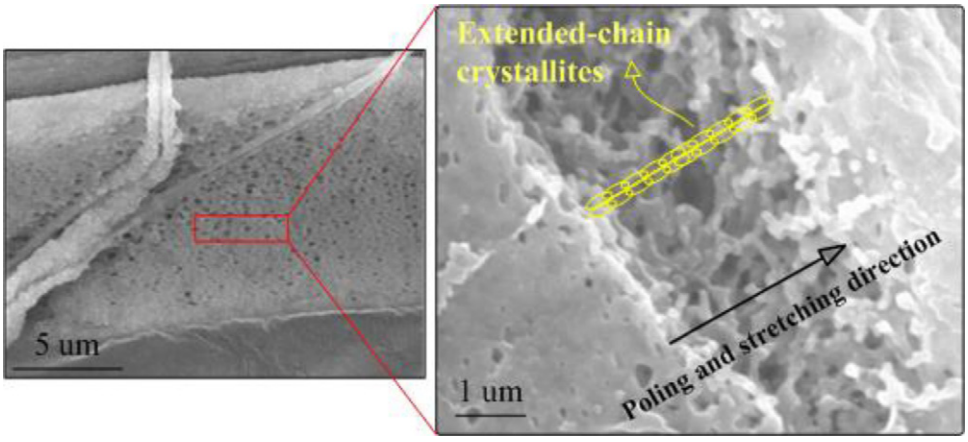

Fig. 12. SEM image of PVDF/MWCNT composite fiber crystal structures.

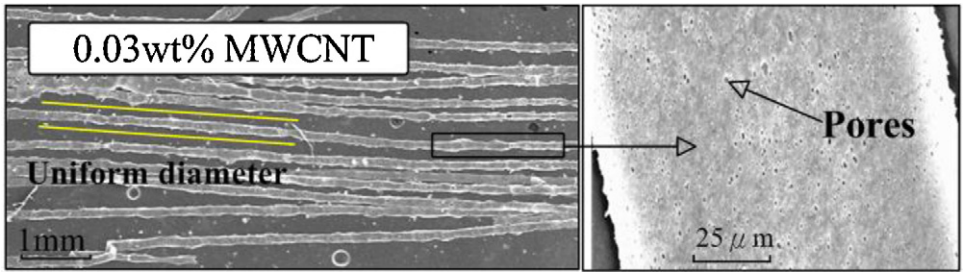

Fig. 13. SEM image of PVDF/MWCNT composite fibers with 0.03 wt% MWCNT.

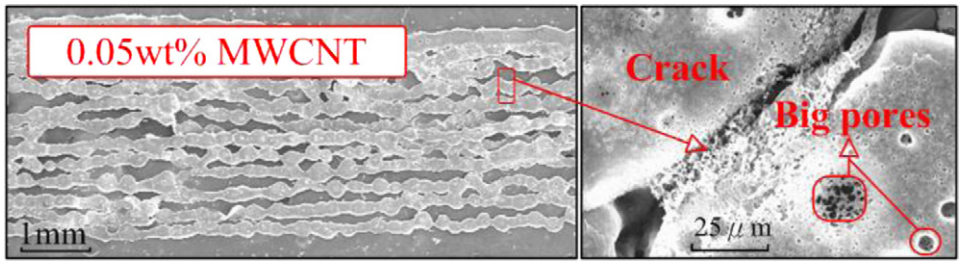

Fig. 14. SEM image of fiber surface morphology after the addition of MWCNT.

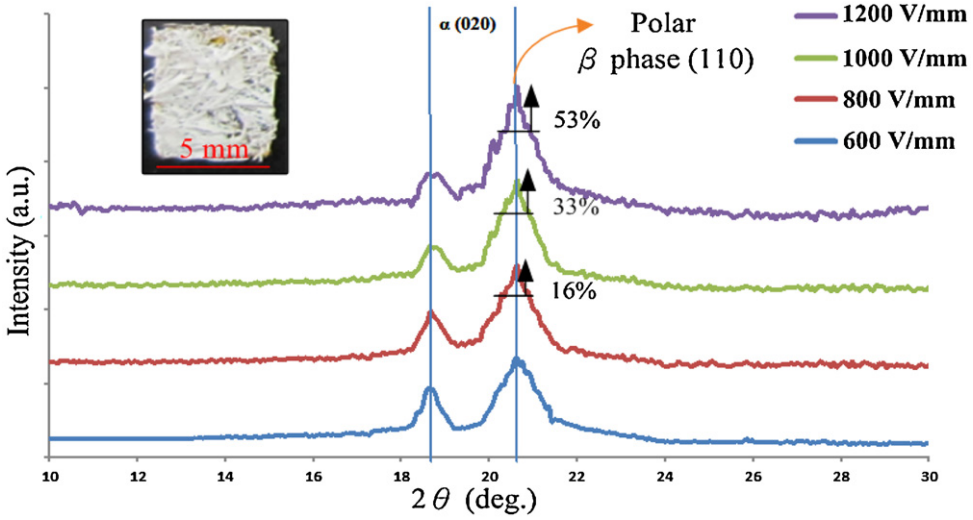

Fig. 15. XRD diffraction patterns of PVDF fibers under different voltages.

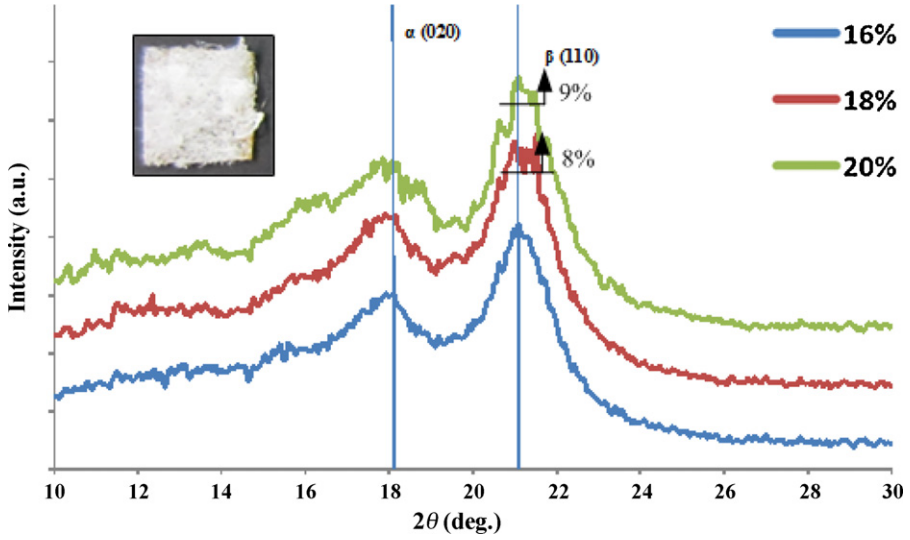

Fig. 16. XRD diffraction patterns of PVDF fibers using different PVDF solution concentrations.

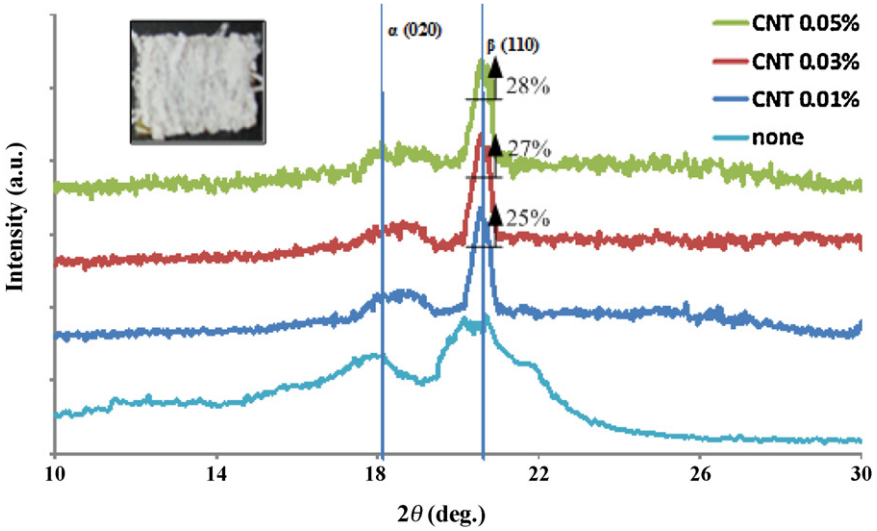

Fig. 17. XRD patterns of PVDF/MWCNT composite nanofibers for different MWCNT concentrations of 0, 0.01, 0.03, and 0.05 wt%, respectively.

MWCNTs were added to the orderly aligned PVDF fibers. MWCNTs may interact with PVDF under the strong extensional force in NFES process, resulting in an obvious β-phase enhancement (Fig. 17). The unique crystalline structures of the PVDF/MWCNT suggested that they arise from the cooperative orientation of the MWCNTs and PVDF chains along the fiber axis, which facilitates the nucleation of highly oriented β-form extended-chain crystallites at the interface [23]. However, piezoelectric properties were not enhanced significantly, despite the addition of MWCNTs to the PVDF fibers. PVDF fibers with non-uniform chain structures on the surface are produced if the MWCNT content of the PVDF solution is 0.05 wt%. To obtain good piezoelectric property and a uniform diameter of PVDF/MWCNT composite fibers, the optimal MWCNT content is 0.03 wt%.

3.4. Analysis of actuation behavior of PVDF fiber with FEM

To investigate the complex piezoelectric responses of the fixed–fixed single PVDF fiber structure under an electric field along the fiber length (z-axis), this study uses the FEA package ANSYS® ver. 11.0 to predict the coupled field behavior. Fig. 18 shows a schematic diagram of the boundary conditions and designed parameters of the fixed–fixed PVDF fiber structure. 3D finite element models of the PVDF fiber were constructed using the SOLID5 3D-coupled field element. Table 2 and appendix list the material parameters with the piezoelectricity of PVDF piezoelectric fiber used in the finite element model. To calculate the center displacement using static analysis, a positive electric field of 1000 V/mm was applied to the fixed–fixed fiber structure. The fiber diameter and length are 10 μm and 1 mm, respectively. Simulation results show a downward center displacement of 5 μm with two significant actuation deformations: the necking phenomenon at the fixed end and compression deformation along the fiber axis. A maximum internal strain appeared in the central part of the PVDF fiber because of the repulsive force and moment near the fixed end. Because the applied polarity of the electric charge was identical to the polarization of the dipole moment, the positive electric field caused compression strain along the fiber axis, making the fiber buckle downward. However, the simulated result and model solution only considered the inverse piezoelectric effect of PVDF fiber,

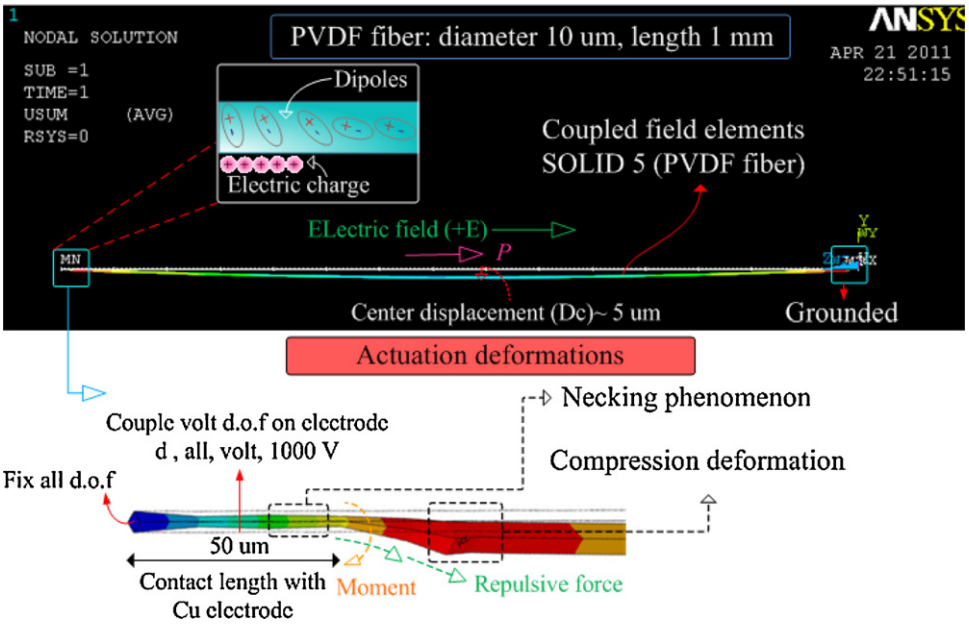

Fig. 18. Simulation results of the deformation of the PVDF fiber.

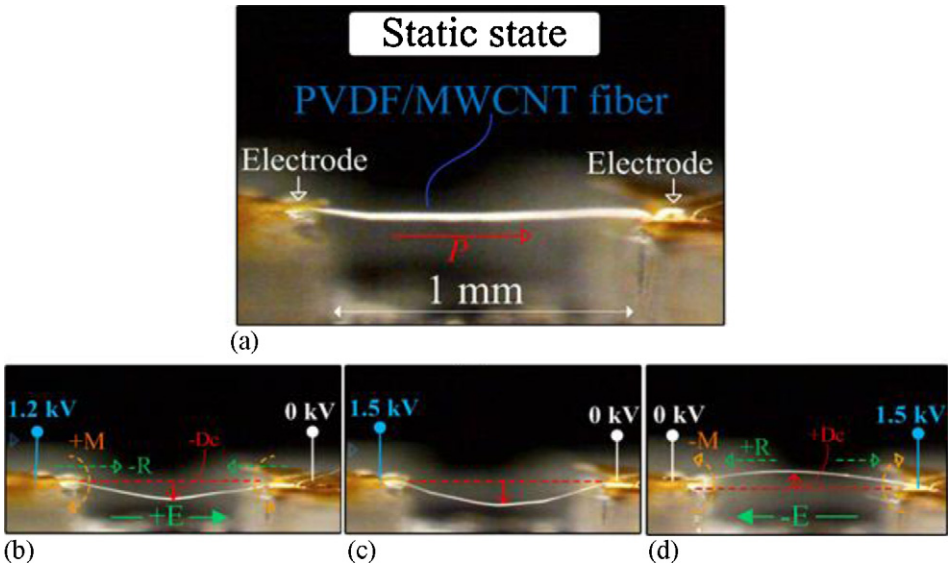

Fig. 19. The deformation of PVDF/MWCNT composite fibers with a 10 μm diameter under various electric fields: (a) static state, (b) 1.2 kV/mm on the left side, (c) 1.5 kV/mm on the left side, (d) 1.5 kV/mm on the right side.

without the electrostatic attraction force induced on the surface of the PVDF fiber (Figs. 21 and 22). Simultaneously investigating the coupled field behaviors, including piezoelectric responses and electrostatic effects of fixed–fixed single PVDF fiber structure under various electric fields, are practically complex. In experiment, the necking phenomenon and compression deformation along the fiber length are difficult to be observed due to deformation dynamics and elasto-plastic behaviors. Therefore, FEA with model solution was employed to assist us in estimating the two significant piezoelectric actuation deformations.

3.5. Observation of PVDF fiber actuator

Based on the fixed–fixed piezoelectric PVDF/MWCNT fiber, Fig. 19 shows the out-of-plane displacement at the central part of an electrospun PVDF fiber under various electric fields (1.2 kV/mm and 1.5 kV/mm on the left side, and 1.5 kV/mm on the right side). Applying an external electric field (+E) along the fiber length produced central displacement downward because the polarity of the electric charge was identical to the polarization of the dipole moment of the piezoelectric fiber (Fig. 19(b) and (c)). A positive electric field (+E) caused a compression strain (−R) along the fiber axis and a moment close to the fixed end, causing the fiber to buckle. Because the applied polarity of the electric charge was opposite to the polarization of the dipole moment, this negative electric field caused insignificant tensile strain (+R) along the fiber axis because of the fixed–fixed beam structure. However, a greater moment (−M) near the fixed end overcame the tensile strain, causing upward center displacement (Fig. 19(d)). The initial deformation caused by the weight of the fiber made the suspended fiber slack [6] (Fig. 19(a)). Therefore, initial deformation was counteracted by the moment on the fixed end, producing a lower upward center displacement. Fig. 20 plots the relationship between the central point displacement of the PVDF fibers and the applied electric field, and shows a comparison of this result with the predicted deformation.

The same electric field was applied to fibers with diameters of 10, 18, and 25 μm. The displacement responses to positive and negative electric fields were in the same direction as the small variation in magnitude. These results are in agreement with the previous theoretical prediction on piezoelectric responses, and show that a thinner fiber with a higher electric field produces a larger displacement.

A positive electric field produced greater displacement. This is because of the accumulated effect of the initial deformation, moment force, and electrostatic attraction force exerted on both ends. Therefore, the observed deformations were higher than predicted. When the fiber was subjected to a higher electric field (1–1.5 kV/mm), the real amount of displacement observed in the fibers produced a greater deviation than predicted. This is because the electrostatic attraction force was more obvious than that at

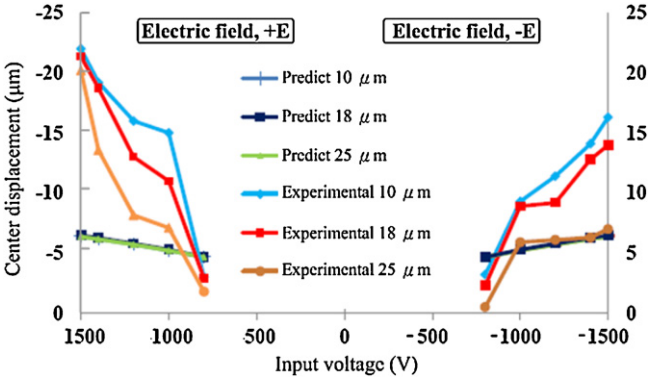

Fig. 20. Center displacement as a function of voltage with various fiber diameters.

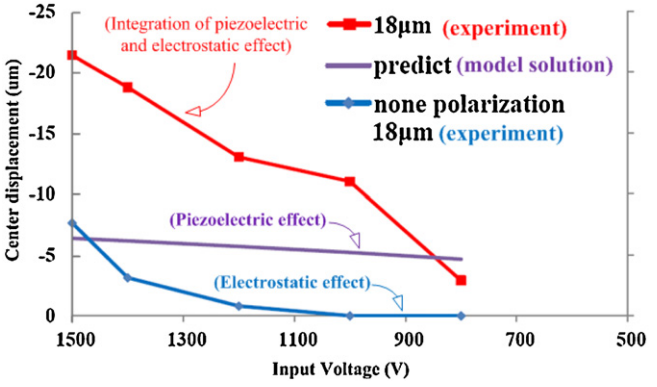

Fig. 21. Center displacement as a function of electric field (+E).

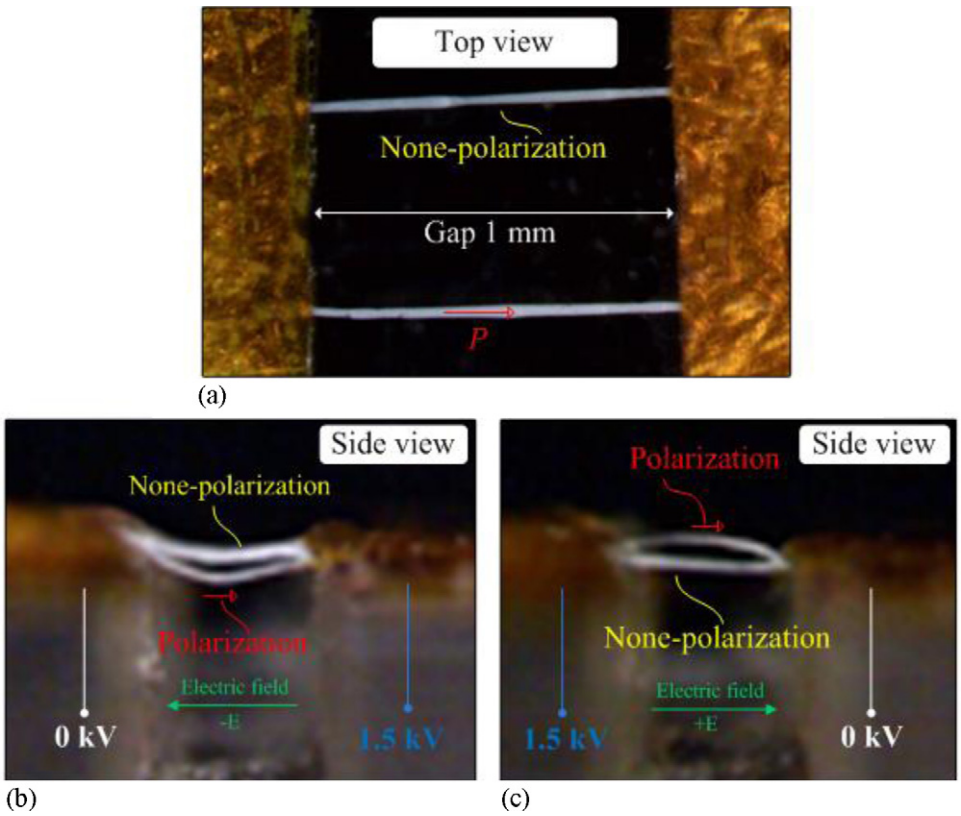

Fig. 22. Center displacement of the non-polarized fiber compared with the polarized fiber in parallel electrodes under a DC voltage supply: (a) the PVDF/MWCNT fiber and PVDF fiber prototypes without polarization, (b) electric field of 1.5 kV/mm on the left side, and (c) electric field of 1.5 kV/mm on the right side.

a lower voltage. The non-polarized fiber was compared with the polarized fiber to determine the electrostatic attraction in this model. Fig. 21 shows the central displacement of the polarized and non-polarized fibers with a 10 μm diameter as a function of voltage under a positive electric field (+*E*). Fig. 22 shows the optical microscopy (OM) observation of the central displacement of polarized and non-polarized fibers under positive and negative electric fields. When a lower electric field was applied, the electrostatic attraction force was insufficient to form an obvious displacement. The total center deformation of the fiber equals the combination of downward electrostatic deformation and downward piezoelectric deformation.

4. Conclusion

This study reports the fabrication of PVDF/MWCNT nanofibers using an NFES technique with fixed–fixed beam structures to easily determine its actuation deformation under various electric fields. The morphology and polarization intensity of piezoelectric fiber can be controlled by adjusting the *X*–*Y* stage velocity, the DC voltage, and the needle-to-collector distance. This study also discusses the optimal parameters of the PVDF solution, including the weight percentage of the PVDF powder and MWCNTs. In addition, the MWCNTs added to the PVDF fibers can increase the crystallinity of the β phase, enhancing piezoelectric properties. XRD analysis of the PVDF fibers with 0.03 wt% MWCNT shows a high diffraction peak at $2\theta = 20.8^{\circ}$, which is characteristic of the piezoelectric crystal β phase. A single piezoelectric PVDF fiber was simulated using ANSYS FEA commercial software with coupled field analysis to determine its center displacement under an applied electric field. Simulation results show two significant deformations: the necking phenomenon at the fixed end and compression deformation along the fiber axis. The actuation property was tested under various electric fields, and the fiber exhibited significant deflection in the experiment. This study describes the center displacements as a function of the electric field for the polarized fiber, non-polarized fiber, and model solution based on a fixed–fixed fiber structure. Results show that the PVDF/MWCNT composite fiber has a downward center displacement of 23 μm and upward center displacement of 16 μm under a high electric field.

Acknowledgements

The authors would like to thank the National Science Council of Taiwan for its financial support under grant NSC-100-2628-E-110-006-MY3. We also sincerely thank National Science Council Core Facilities Laboratory for Nano-Science and Nano-Technology in National Sun Yat-Sen University, Kaohsiung-Pingtung area, Taiwan for supports.

Appendix A. The parameters on piezoelectricity of PVDF fiber

PVDF "compliance" matrix [*s*]

$$[s]^E = \begin{Bmatrix} 385 & -165 & -165 & 0 & 0 & 0 \\ -165 & 385 & -165 & 0 & 0 & 0 \\ -165 & -165 & 385 & 0 & 0 & 0 \\ 0 & 0 & 0 & 1330 & 0 & 0 \\ 0 & 0 & 0 & 0 & 1330 & 0 \\ 0 & 0 & 0 & 0 & 0 & 1330 \end{Bmatrix} \times 10^{-12} \ (\mathrm{m^2/N})$$

PVDF "piezoelectric strain" matrix [d] [6,20]

$$[d] = \begin{Bmatrix} 0 & 0 & 0 & 0 & 0 & 0 \\ 0 & 0 & 0 & 0 & 0 & 0 \\ 20 & 3 & -46 \pm 14 & 0 & 0 & 0 \end{Bmatrix} \times 10^{-12} \quad (\mathrm{m/V})$$

PVDF "dielectric Matrix" [ε^T]

$$[\varepsilon^T] = \begin{Bmatrix} 9 & 0 & 0 \\ 0 & 9 & 0 \\ 0 & 0 & 9 \end{Bmatrix} \times 8.854 \times 10^{-12} \quad (\mathrm{F/m})$$

References

[1] X. Chen, S.Y. Xu, N. Yao, Y. Shi, 1.6 V Nanogenerator for mechanical energy harvesting using PZT nanofibers, Nano Letters 10 (6) (2010) 2133–2137.
[2] A.G. Holmes-Siedle, P.D. Wilson, A.P. Verrall, PVDF: an electronically-active polymer for industry, Materials & Design 4 (6) (1984) 910–918.
[3] T. Sato, H. Ishikawa, O. Ikeda, Multilayered deformable mirror using PVDF films, Applied Optics 21 (20) (1982) 3664–3668.
[4] J.M. Ha, H.O. Lim, N.J. Jo, Actuation behavior of CP actuator based on polypyrrole and PVDF, Advanced Materials Research 29 (2007) 363–366.
[5] C. Chang, Y.K. Fuh, L. Lin, A direct-write piezoelectric PVDF nanogenerator, in: 15th International Conference on Solid-State Sensors, Actuators and Microsystems, Denver, pp. 1485–1488, 2009.
[6] J. Pu, X. Yan, Y. Jiang, C. Chang, L. Lin, Piezoelectric actuation of direct-write electrospun fibers, Sensors and Actuators A: Physical 164 (1) (2010) 131–136.
[7] M.C. Celina, T.R. Dargaville, P.M. Chaplya, R.L. Clough, Piezoelectric PVDF materials performance and operation limits in space environments, Materials Research Society Proceedings 851 (2005) 449–460.
[8] W.A. Yee, M. Kotaki, Y. Liu, X. Lu, Morphology, polymorphism behavior and molecular orientation of electrospun poly(vinylidene fluoride) fibers, Polymer 48 (2) (2007) 512–521.
[9] A. Theron, E. Zussman, A.L. Yarin, Electrostatic field-assisted alignment of electrospun nanofibers, Nanotechnology 12 (3) (2001) 384–390.
[10] D.H. Reneker, A.L. Yarin, H. Fong, S. Koombhongse, Bending instability of electrically charged liquid jets of polymer solutions in electrospinning, Journal of Applied Physics 87 (9) (2000) 4531–4547.
[11] S.F. Fennessey, R.J. Farris, Fabrication of aligned and molecularly oriented electrospun polyacrylonitrile nanofibers and the mechanical behavior of their twisted yarns, Polymer 45 (12) (2004) 4217–4225.
[12] K.W. Kim, K.H. Lee, M.S. Khil, Y.S. Ho, H.Y. Kim, The effect of molecular weight and the linear velocity of drum surface on the properties of electrospun poly(ethylene terephthalate) nonwovens, Fibers and Polymers 5 (2) (2004) 122–127.
[13] D. Li, Y. Wang, Y. Xia, Electrospinning of polymeric and ceramic nanofibers as uniaxially aligned arrays, Nano Letters 3 (8) (2003) 1167–1171.
[14] S.A. Theron, E. Zussman, A.L. Yarin, Experimental investigation of the governing parameters in the electrospinning of polymer solutions, Polymer 45 (6) (2004) 2017–2030.
[15] D. Sun, C. Chang, S. Li, L.W. Lin, Near-field electrospinning, Nano Letters 6 (4) (2006) 839–842.
[16] C. Chang, K. Limkrailassiri, L.W. Lin, Continuous near-field electrospinning for large area deposition of orderly nanofiber patterns, Applied Physics Letters 93 (12) (2008) 123111.
[17] C. Chang, V.H. Tran, J. Wang, Y.K. Fuh, L.W. Lin, Direct-write piezoelectric polymeric nanogenerator with high energy conversion efficiency, Nano Letters 10 (2010) 726–731.
[18] Y.J. Zhang, Z.D. Zhao, W.X. Yu, Preparation and characterizations of PVDF/MWCNT nanocomposites, Polymer Materials Science and Engineering 26 (6) (2010) 141–144.
[19] R. He, X.L. Feng, M.L. Roukes, P. Yang, Self-transducing silicon nanowire electromechanical systems at room temperature, Nano Letters 8 (6) (2008) 1756–1761.
[20] J. Pu, X. Yan, Y. Jiang, C. Chang, L. Lin, Piezoelectric actuation of a direct write electrospun PVDF fiber, in: Micro Electro Mechanical Systems (MEMS), 2010 IEEE 23rd International Conference, 2010, pp. 1163–1166.
[21] S.Y. Gu, Q.L. Wu, J. Ren, G. Julius Vancso, Mechanical properties of a single electrospun fiber and its structures, Macromolecular Rapid Communications 26 (9) (2005) 716–720.
[22] H. Ye, H. Lam, N. Titchenal, Y. Gogotsi, F. Ko, Reinforcement and rupture behavior of carbon nanotubes–polymer nanofibers, Applied Physics Letters 85 (10) (2004) 1775–1777.
[23] S. Huang, W.A. Yee, W.C. Tjiu, Y. Liu, M. Kotaki, Y.C.F. Boey, J. Ma, T. Liu, X. Lu, Electrospinning of polyvinylidene difluoride with carbon nanotubes: synergistic effects of extensional force and interfacial interaction on crystalline structures, Langmuir 24 (2008) 13621–13626.

Biographies

Dr. Z.H. Liu was born in Kaohsiung, Taiwan, Republic of China, in 1981. He received his engineering degree of master and doctor in 2009 and 2012, respectively, from Department of Mechanical and Electro-Mechanical Engineering of National Sun-Yat-Sen University in Kaohsiung, Taiwan. His current research interests focus on thin-film process, piezoelectric nanomaterials, flexible electronics composites, energy harvesting.

Professor C.T. Pan was born in Nauto, Taiwan, in 1969. He received his engineering degree of master and doctor in 1993 and 1998, respectively, from Power Mechanical Engineering Department of National Tsing Hua University in Hsinchu, Taiwan. He was a researcher in the field of laser machining polymer in the TU Berlin (IWF) in Germany from 1997 to 1998 and a researcher of MEMS Division in the MIRL/ITRI, Hsinchu in Taiwan from 1998 to 2003. He joined National Sun Yat-Sen University, Kaohsiung, Taiwan, as an assistant professor in 2003 and earned his professorship in 2008. His current research interests focus on MEMS, NEMS, and LIGA process.

Professor L.W. Lin currently serves as Chancellor's Professor of the Department of Mechanical Engineering at the University of California at Berkeley, and Co-Director of the Berkeley Sensor and Actuator Center. Professor Lin received his B.S. (1986) in power mechanical engineering from the National Tsing Hua University in Taiwan, and then received his M.S. (1991) and Ph.D. (1993) degrees from UC Berkeley in mechanical engineering. After graduation, Professor Lin held the position of senior research scientist at BEI Electronics Inc. He also served as associate professor at the National Taiwan University and assistant professor at the University of Michigan before joining the faculty at UC Berkeley in 1999. Professor Lin also held the position of vice chair of graduate study within the mechanical engineering department from 2006–2009. Professor Lin's research interests and activities at UC Berkeley include MEMS, NEMS, Nanotechnology, design and manufacturing of microsensors and microactuators, development of micromachining processes by silicon surface/bulk micromachining, micro molding process, and mechanical issues in MEMS such as heat transfer, solid/fluid mechanics and dynamics. Professor Lin is the co-inventor listed on 14 patents in MEMS and has authored or co-authored 90 journal publications and more than 130 refereed conference proceedings. Since 1996 he has graduated 17 Ph.D. and 25 M.S. students.

H.W. Lai was born in Taichung, Taiwan, Republic of China, in 1986. He received his received B.S. and M.S. degrees in 2009 and 2011, respectively, from Department of Mechanical and Electro-Mechanical Engineering of National Sun-Yat-Sen University in Kaohsiung, Taiwan. His current research interests focus on PVDF nanofiber fabrication and near-field electrospinning process.